Journal of Medicinal Chemistry

pubs.acs.org/jmc Article

Hydroxamate-Based Selective Macrophage Elastase (MMP-12) Inhibitors and Radiotracers for Molecular Imaging

Kiran Gona, Jakub Toczek, Yunpeng Ye, Nowshin Sanzida, Arvene Golbazi, Parnaz Boodagh, Mani Salarian, Jae-Joon Jung, Saranya Rajendran, Gunjan Kukreja, Terence L. Wu, Laurent Devel, and Mehran M. Sadeghi*

Cite This: https://dx.doi.org/10.1021/acs.jmedchem.0c01514 Read Online

ACCESS | Metrics & More | Article Recommendations | Supporting Information

ABSTRACT: Macrophage elastase [matrix metalloproteinase (MMP)-12] is the most upregulated MMP in abdominal aortic aneurysm (AAA) and, hence, MMP-12-targeted imaging may predict AAA progression and rupture risk. Here, we report the design, synthesis, and evaluation of three novel hydroxamate-based selective MMP-12 inhibitors (CGA, CGA-1, and AGA) and the methodology to obtain MMP-12 selectivity from hydroxamate-based panMMP inhibitors. Also, we report two ^{99m}Tc-radiotracers, ^{99m}Tc-AGA-1 and ^{99m}Tc-AGA-2, derived from AGA. ^{99m}Tc-AGA-2 displayed faster blood clearance in mice and better radiochemical stability compared to ^{99m}Tc-AGA-1. Based on this, ^{99m}Tc-AGA-2 was chosen as the lead tracer and tested in murine AAA. ^{99m}Tc-AGA-2 uptake detected by autoradiography was significantly higher in AAA compared to normal aortic regions. Specific binding of the tracer to MMP-12 was demonstrated through ex vivo competition. Accordingly, this study introduces a novel family of selective MMP-12 inhibitors and tracers, paving the way for further development of these agents as therapeutic and imaging agents.

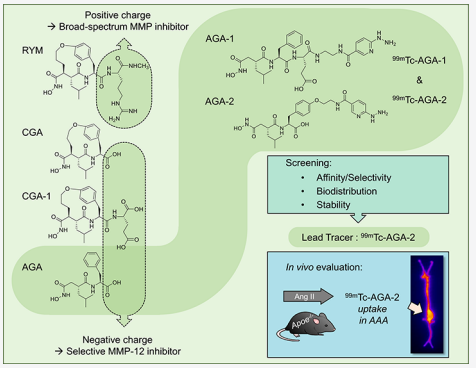

INTRODUCTION

Matrix metalloproteinases (MMPs) are calcium-dependent zinc endopeptidases that belong to the family of metzincins. These enzymes are capable of degrading different components of the extracellular matrix (ECM),[1] the regulated breakdown of which is essential for many biological processes, including tissue remodeling and resorption.[2−4] Dysregulated ECM degradation contributes to a wide range of diseases such as cancer, arthritis, nephritis, heart failure, atherosclerosis, and aneurysm.[5−12] MMPs also participate in pathophysiological processes by regulating the release or activation of chemokines, cytokines, growth factors, and other bioactive molecules.[13−15] Typically, MMPs are secreted as inactive zymogens and require proteolytic activation by tissue or plasma proteinases to become active. MMP activity is also regulated by endogenous regulators called tissue inhibitors of metalloproteinases. Owing to their important role, MMPs are considered as promising targets for the development of new therapeutic and diagnostic tools. Based on this, several broad-spectrum MMP inhibitors (MMPIs) have been developed as therapeutic agents.[6,16−19] In addition, single-photon emission computed tomography (SPECT) and positron emission tomography (PET) tracers are under development and evaluation in preclinical animal models for molecular imaging of cardiovascular and other diseases.[20−22] Several MMPIs have failed as therapeutic agents in late-phase clinical trials, mainly due to musculoskeletal side effects, possibly related to their lack of selectivity and the complexity of their actions.[19] These drawbacks can be potentially overcome by developing more selective MMP inhibitors.

MMP-12 or macrophage elastase, a 55 kDa protein best known for its elastase activity, is produced by macrophages and a number of other cell types.[23] MMP-12 is implicated in the pathogenesis of abdominal aortic aneurysm (AAA). While normal arteries express low levels of MMP-12, it is highly upregulated in aneurysmal arteries in humans and animal models of AAA.[24−26] Accordingly, selective MMP-12 targeting may be a potential therapeutic, as well as molecular imaging target in this setting.[23,25,27,28]

Several hydroxamate-based succinic acid derivatives with α, P1′, P2′, and P3′ substituents have been developed as panMMP inhibitors, where the hydroxamate group acts as a zinc binding group (ZBG).[22,29−33] The structure−activity relationship experiments performed on these series but also those on other series of MMPIs have elucidated the structural

Received: September 26, 2020

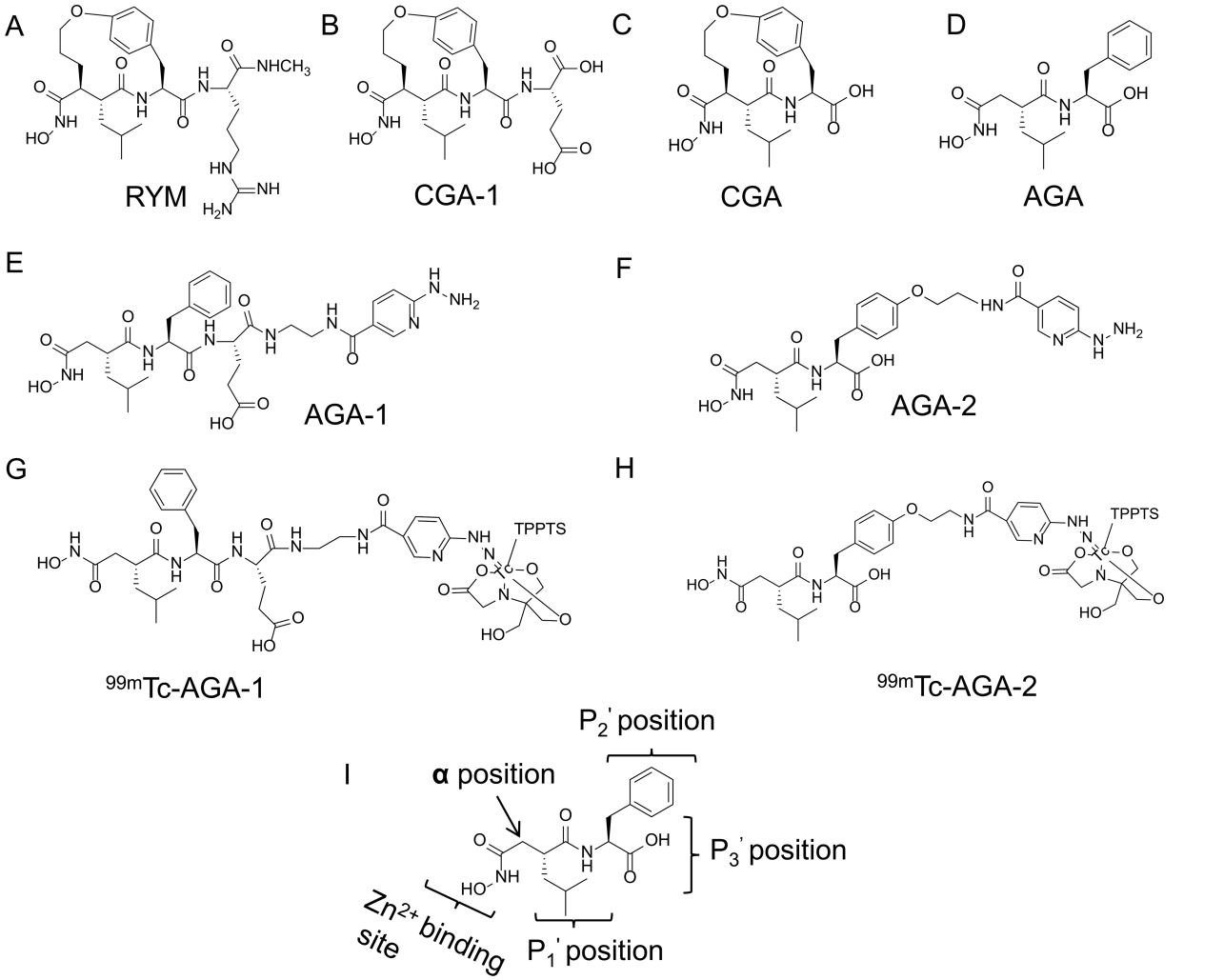

Figure 1. Chemical structures of the panMMP inhibitor RYM (A) and novel cyclic MMP-12 inhibitors CGA-1 (B) and CGA (C), as well as the novel acyclic MMP-12 inhibitor AGA (D), radiolabeling precursors AGA-1 (E) and AGA-2 (F), and their corresponding ^{99m}Tc-labeled SPECT imaging agents ^{99m}Tc-AGA-1 (G) and ^{99m}Tc-AGA-2 (H). The key structural components of AGA and the structure−activity relationship used to develop novel selective MMP-12 inhibitors and SPECT imaging agents are shown in (I).

requirements to achieve potency and selectivity. In this respect, the hydroxamate function as a strong ZBG mainly drives MMPI potency, while the side chain at the P1′ segment, which interacts within the hydrophobic S1′ pocket, allows the modulation of their selectivity, with significant differences when the length and flexibility of this side chain are modified. The impact of P1′ on MMPI selectivity is even more pronounced when weaker ZGBs than the hydroxamate moiety are used.[34] Similarly, substituents at α, P2′, and P3′ positions have often minimal effects in hydroxamate series but have more impact when other ZBGs are employed. Accordingly, two glutamate residues in P2′ and P3′ positions within a pseudo-peptide scaffold containing a phosphinic function as a weak ZBG and clearly drive the inhibitor selectivity for MMP-12.[35,36] However, our recent studies on the complex role of the ZBG[36] clearly showed that subtle modulations between the latter and the different substituents along the pseudo-peptide backbone have to be carefully considered to achieve selectivity, not excluding the possibility to identify selective binders in the hydroxamate series.

Given the role of MMP-12 in AAA and other pathological processes, we have sought to develop selective MMP-12 inhibitors and their corresponding radiotracers with a considerable selectivity over other metalloproteinases. Anti-succinate-based acyclic or cyclic hydroxamate analogues have been extensively studied in the literature as panMMP inhibitors and their chemistry is well established. While keeping the hydrophobic P1′ fragment unchanged on the anti-succinate hydroxamate core, cyclizing the α and P2′ positions, and modifying the P3′ segment with a free acid side chain (CGA and CGA-1, Figure 1), we observed selective binding toward MMP-12 when compared with several other MMPs. Keeping in mind the challenges involved in preparing these multistep, multichiral cyclic analogues, a similar methodology (keeping a free acid side chain) was used to prepare an easily accessible succinyl hydroxamate-based acyclic analogue (AGA, Figure 1), which also displayed selective MMP-12 inhibition. Two precursors for ^{99m}Tc conjugation (AGA-1 and AGA-2, Figure 1) developed based on AGA retained MMP-12 selectivity. The corresponding single-photon computed tomography (SPECT) tracers (^{99m}Tc-AGA-1 and ^{99m}Tc-AGA-2, Figure 1) were synthesized and their radiochemical stability, ex vivo binding, pharmacokinetics, and biodistribution were evaluated and compared. Finally, the tracer displaying the best performance, ^{99m}Tc-AGA-2, was tested in a murine model of AAA in which MMP-12 is upregulated.

https://dx.doi.org/10.1021/acs.jmedchem.0c01514
J. Med. Chem. XXXX, XXX, XXX−XXX

Scheme 1. Synthetic Scheme for the Preparation of CGA and CGA-1[a]

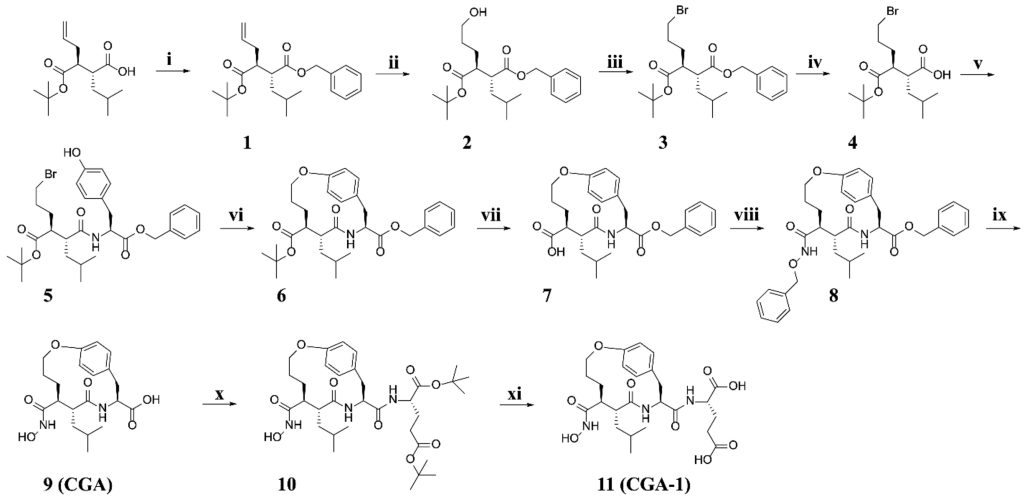

[a]Reagents and conditions: i. BnBr/DBU/toluene/RT/2 h and 60 °C/1 h/71% yield; ii. (a) 9-BBN/THF; (b) H_2O_2/H_2O/RT/12 h/70% yield; iii. CBr_4/Ph_3P/DCM/RT/63% yield; iv. Pd/C (10%)/H_2/CH_3OH/RT/30 min/85% yield; v. *H*-Tyr-*O*Bz/EDCI/HOBT/DMF/RT/12 h/74% yield; vi. Cs_2CO_3/acetonitrile/RT/6 h/55% yield; vii. TFA/DCM/RT/2 h/100% yield; viii. Bz-ONH_2/HOAT/HATU/DIPEA/DMF/RT/18 h/62% yield; ix. Pd/C (10%)/H_2/CH_3OH/RT/2 h/58% yield; x. Glu-di-*t*-butyl ester/EDCI/HOBT/DMF/RT/18 h/25% yield; xi. TFA/DCM/RT/2 h/8% yield.

RESULTS

Synthesis of Selective MMP-12 Inhibitors. The synthetic strategy used for the preparation of CGA and CGA-1 is shown in Scheme 1. The anti-succinic acid derivative (2*R*,3*S*)-3-(*tert*-butoxycarbonyl)-2-isobutylhex-5-enoic acid was used as the starting material and converted into its benzyl ester (**1**) using 1,8-diazabicyclo[5.4.0]undec-7-ene (DBU) and benzyl bromide in toluene. The intermediate **2** was prepared by hydroboration of **1** using 9-borabicyclo[3.3.1]nonane (9-BBN) and H_2O_2 in tetrahydrofuran (THF). The hydroxyl intermediate (**2**) was converted into its bromide derivative using CBr_4 and triphenylphosphine (Ph_3P) in dichloromethane (DCM) to obtain **3**. The benzyl ester group on **3** was deprotected using 10% palladium on carbon (Pd/C) and hydrogen gas in methanol to obtain **4**. L-Tyrosine benzyl ester was coupled to the acid **4** using 1-ethyl-3-(3-dimethylaminopropyl) carbodiimide hydrochloride (EDCI) and 1-hydroxybenzotriazole hydrate (HOBT) in *N*,*N*-dimethyl formamide (DMF) to obtain **5**. The bromo group from the α-position and the hydroxyl group from P_2' were cyclized using Cs_2CO_3 in anhydrous acetonitrile to give the cyclized intermediate **6**. The *t*-butyl group on **6** was deprotected using trifluoroacetic acid (TFA) in DCM to obtain **7**, which was coupled with *O*-benzyl hydroxylamine hydrochloride using HBTU in DMF to obtain **8**. Both benzyl groups on **8** were deprotected using 10% Pd/C and hydrogen gas in methanol to obtain the acid CGA (**9**). Coupling of L-glutamic acid di-*tert*-butyl ester with **9** using EDCI and HOBT in DMF followed by hydrolysis of acid esters resulted in CGA-1 (**11**).

The synthetic strategy used for the preparation of AGA and AGA-1 is shown in Scheme 2. The synthesis started from 4-methylpentanoic acid, which was converted to 4-methylpentanoyl chloride using oxalyl chloride in THF at 0 °C. The acid chloride obtained was then converted to intermediate **12** by reacting with (*S*)-(−)-4-benzyl-2-oxazolidinone in THF at −78 °C. Reacting intermediate **12** with 2.0 M sodium bis(trimethylsilyl)amide solution (NaHMDS) at −78 °C followed by *tert*-butyl bromoacetate in THF resulted in **13**. The hydrolysis of **13** using a 30% hydrogen peroxide solution and LiOH-H_2O in THF/H_2O at 0 °C resulted in **14**. L-Phenylalanine-*O*Bz ester was coupled with intermediate **14** using EDCI and HOBT in DMF to obtain **15**. The *t*-butyl group of intermediate **15** was hydrolyzed using TFA in DCM to result in **16**. The acid obtained was coupled with *O*-benzyl hydroxylamine hydrochloride using EDCI and HOBT in DMF to result in intermediate **17**. Both benzyl groups on **17** were deprotected using 10% Pd/C and hydrogen gas in methanol to obtain AGA (**18**).

The Fmoc-L-glutamate benzylester was coupled with *N*-Boc-ethylenediamine using EDCI and HOBT in DMF to obtain **19**. Deprotection of the Boc-protecting group using TFA and DCM resulted in **20**, which was coupled with 6-Boc-hydrazinonicotinic acid (Boc-HYNIC acid) to obtain **21**. The Fmoc group was deprotected using piperidine in DCM to obtain intermediate **22**, which was coupled with intermediate **18** using EDCI and HOBT in DMF to obtain **23**. The benzyl ester was hydrolyzed using 10% Pd/C and hydrogen gas in methanol and deprotection of *N*-Boc using TFA in DCM resulted in AGA-1 (**24**).

The synthetic strategy used for the preparation of AGA-2 is shown in Scheme 3. D-Tyrosine alanine *O*-benzyl ester was coupled with the intermediate **14** using EDCI and HOBT in DMF to obtain **25**. The *t*-butyl group of **25** was hydrolyzed using TFA in DCM and led to **26**. The resulting acid was coupled with *O*-benzyl hydroxylamine hydrochloride using EDCI and HOBT in DMF to access **27**. *N*-Boc-protected ethanolamine was coupled with **27** using Cs_2CO_3 in DMF to obtain **28**. The *N*-Boc group was deprotected using TFA in DCM to obtain **29**, which was coupled with *N*-Boc-protected HYNIC acid using HATU and HOAT in DMF to obtain **30**. The *N*-Boc group was deprotected using TFA in DCM to obtain **31**, which following deprotection of di-benzyl groups using 10% Pd/C under hydrogen gas, resulted in AGA-2 (**32**).

MMP Affinity Determination. The inhibition constants (K_i) of CGA, CGA-1, and AGA, as well as the radiolabeling precursors AGA-1 and AGA-2 were evaluated in comparison

https://dx.doi.org/10.1021/acs.jmedchem.0c01514
J. Med. Chem. XXXX, XXX, XXX−XXX

Scheme 2. Synthetic Scheme for the Preparation of AGA and AGA-1[a]

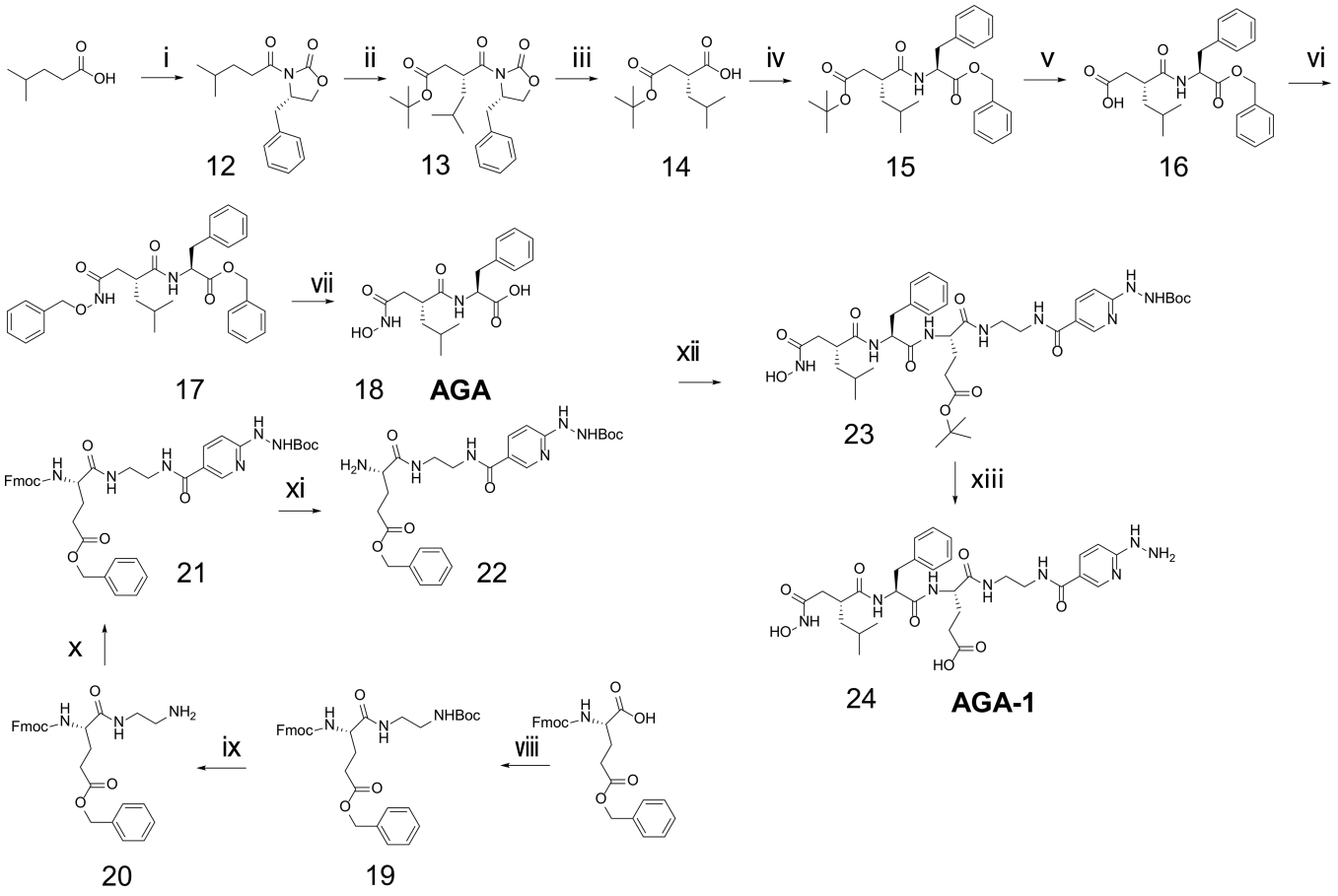

[a]Reagents and conditions: i. pivCl/LiCl/0 °C/2 h/*S*-benzyl oxazolidinone/THF/−78 °C to RT/12 h/55% yield; ii. NaHMDS (1.9 M)/Br-CH_2CO_2-*t*-Bu/THF/−78 °C to RT/12 h/62% yield; iii. LiOH/H_2O_2/THF/0 °C to RT/2 h/75% yield; iv. L-phenylalanine benzyl ester/EDCI/HOBT/DMF/RT/18 h/72% yield; v. TFA/DCM/RT/2 h/100% yield; vi. Bz-ONH_2/BOP/DIEA/DMF/RT/18 h/80% yield; vii. Pd/C (10%)/H_2/CH_3OH/RT/2 h/62% yield; viii. Boc-NH-CH_2CH_2-NH_2/Fmoc-Glu(*O*-Bz)-OH/EDCI/HOBT/DMF/0 °C to RT/2.5 h/72% yield; ix. TFA/DCM/RT/30 min/72% yield; x. *N*-Boc-HYNIC acid/EDCI/HOBT/DIEA/DMF/RT/18 h/55% yield; xi. piperidine/DCM/RT/30 min/65% yield; xii. 2.7/2.11/EDCI/HOBT/DIPEA/DMF/RT/18 h/45% yield; xiii. (a) TFA/DCM/RT/2 h; (b) Pd/C (10%)/H_2/CH_3OH/RT/2 h/14% yield.

Scheme 3. Synthetic Scheme for the Preparation of AGA-2[a]

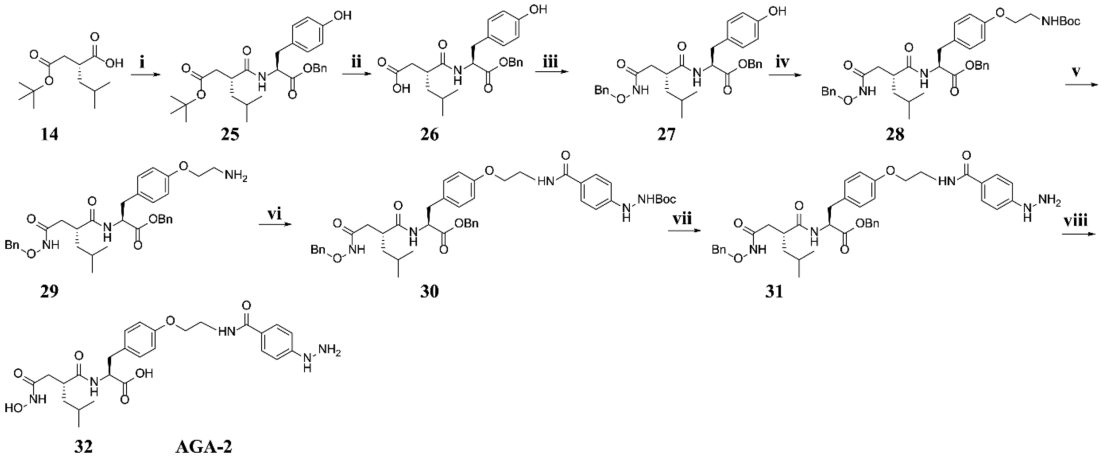

[a]Reagents and conditions: i. *H*-Tyr-*O*Bz/EDCI/HOBT/DMF/RT/18 h/65% yield; ii. TFA/DCM/RT/2 h/100% yield; iii. Bz-ONH_2/HBTU/DIEA/DMF/RT/18 h/66% yield; iv. 2-(BOC-amino)ethyl bromide/Cs_2CO_3/acetonitrile/60 °C/4 h/58% yield; v. TFA/DCM/RT/2 h/100% yield; vi. *N*-Boc-HYNIC acid/HOAT/HATU/DIEA/DMF/RT/18 h/53% yield; vii. TFA/DCM/RT/100% yield; viii. Pd/C (10%)/H_2/CH_3OH/RT/2 h/9% yield.

https://dx.doi.org/10.1021/acs.jmedchem.0c01514
J. Med. Chem. XXXX, XXX, XXX−XXX

Table 1. Inhibition Constants (K_i) of AGA, CGA, CGA-1, and RYM[a]

K_i (nM)	rhMMP-2	rhMMP-7	rhMMP-9	rhMMP-12	rhMMP-13
CGA	300 ± 81	39 ± 2.0	1101 ± 289	1.1 ± 0.6	31 ± 12
CGA-1	396 ± 28	14.6 ± 0.1	2107 ± 454	1.2 ± 0.1	89 ± 18
RYM	5.8 ± 0.4	17.2 ± 0.1	20.4 ± 2.0	1.0 ± 0.5	15.3 ± 5.4
AGA	164 ± 43	323 ± 129	125 ± 14	11.8 ± 1	81 ± 33
AGA-1	222 ± 17	615 ± 53	1305 ± 204	7.5 ± 1.4	78 ± 5
AGA-2	>5 μM	>5 μM	155 ± 14	8.9 ± 0.2	>5 μM

[a] K_i values represent the mean ± SD of three experiments.

with the panMMP inhibitor RYM for a set of recombinant human MMPs (rhMMPs) using an assay involving the cleavage of a fluorogenic substrate, Mca-Lys-Pro-Leu-Gly-Leu-Dpa-Ala-Arg-NH_2. All newly developed inhibitors showed great affinity and selectivity toward rhMMP-12 when compared to a select group of rhMMPs. Accordingly, the cyclic inhibitors CGA and CGA-1 displayed K_i values of <2 nM, and acyclic inhibitors AGA, AGA-1, and AGA-2 displayed K_i values ranging from 7.5 to 12 toward rhMMP-12 (Table 1). The selectivity of cyclic inhibitors for rhMMP-12 relative to other MMPs tested ranged from at least 12-fold (for CGA-1 against rhMMP-7) to 28-fold (for CGA against rhMMP-13). Among acyclic inhibitors, AGA-2 displayed the highest selectivity (17-fold against rhMMP-9). Finally, like their binding to rhMMP-12, all inhibitors showed high affinity for murine MMP-12 (Table S1).

Radiolabeling. ^{99m}Tc-labeling of precursors AGA-1 and AGA-2 was performed according to an established methodology.[37,38] Both ^{99m}Tc-AGA-1 and ^{99m}Tc-AGA-2 showed more than 95% conversion of $^{99m}TcO_4^-$ to its radiolabeling product with retention times of 18.0 and 22.6 min, respectively. Both ^{99m}Tc-AGA-1 and ^{99m}Tc-AGA-2 were consistently obtained with >95% radiochemical yield and radiochemical purity without a need for any purification. To further confirm the radiolabeling efficiency, when AGA-1 or AGA-2 (HYNIC precursors) was not added to the labeling solution, only one major peak of ^{99m}Tc-colloid or ^{99m}Tc-coligand product at 3.3 min was observed, and there was no radioactive peak corresponding to radiolabeled products at 18.0 or 22.6 min (Figure S1). The specific activity values of the radiotracers were in the range of 540−810 MBq/nmol.

Binding to Human AAA Tissue. MMP-12 is highly upregulated in human AAA and several preclinical studies have indicated its important role in the development and potentially rupture of AAA.[22,24−26,39] Therefore, as a prelude to performing in vivo imaging studies, we evaluated the binding of ^{99m}Tc-AGA-1 and ^{99m}Tc-AGA-2 to human AAA and normal aorta. Both ^{99m}Tc-AGA-1 and ^{99m}Tc-AGA-2 displayed significantly higher binding to human AAA as compared to normal aortic tissue (P < 0.001 for ^{99m}Tc-AGA-1 and P < 0.001 for ^{99m}Tc-AGA-2, n = 3 per group, Figure 2).

Radiotracer Biodistribution. The biodistribution and blood clearance of ^{99m}Tc-AGA-1 and ^{99m}Tc-AGA-2 were investigated in C57BL/6J mice following intravenous administration of each radiotracer (18.5 ± 3.7 MBq). These and other animal studies were performed under protocols approved by Yale University and Veteran Affairs Connecticut institutional animal care and use committees. Serial blood samples were collected over a 2 h period, following which the animals were euthanized, different tissue samples and body fluids were collected and weighed, and their radioactivity was measured by gamma-well counting. Relative to ^{99m}Tc-AGA-1, ^{99m}Tc-AGA-2

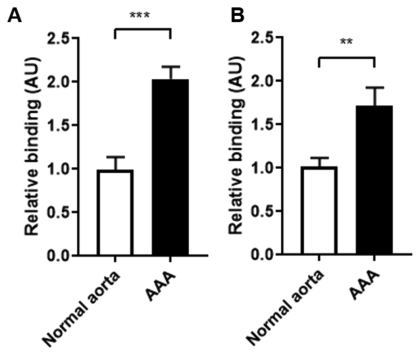

Figure 2. Ex vivo binding of ^{99m}Tc-AGA-1 (A) and ^{99m}Tc-AGA-2 (B) to human normal aorta and AAA tissue. n = 3 in each group; $^{**}P$ < 0.01 and $^{***}P$ < 0.001. AU, arbitrary units.

showed faster blood clearance with a residual blood level of 1.2 ± 0.2% injected dose (ID)/mL at 2 h post injection (p.i.), while the residual blood activity for ^{99m}Tc-AGA-1 was 3.0 ± 0.2% ID/mL at 2 h p.i. (Figure 3). The high activity in bile and kidney indicated mixed hepatobiliary and renal clearance for both tracers. Importantly, both tracers displayed low uptake (2.0 ± 0.4 and 2.0 ± 0.9% ID/g, respectively) in the normal aorta, supporting the possibility of using these tracers for vascular imaging applications (Figure 3).

Stability Studies. ^{99m}Tc-AGA-1 and ^{99m}Tc-AGA-2 were incubated in murine blood at 37 °C and their stability was monitored by radio-HPLC analysis at 1 and 2 h post incubation. ^{99m}Tc-AGA-1 exhibited poor stability, with the radio-HPLC peak corresponding to the intact tracer decreasing to ∼70% of total radioactivity at 1 h and ∼50% of that activity at 2 h. Conversely, ^{99m}Tc-AGA-2 showed excellent radiochemical stability during the 2 h blood incubation period (Figure 4).

Evaluation in Murine Model of AAA. Based on its favorable selectivity, pharmacokinetics, and stability in blood, ^{99m}Tc-AGA-2 was selected for further evaluation in a murine model of AAA that is associated with significant MMP-12 upregulation. Apolipoprotein E-deficient ($Apoe^{-/-}$) mice (n = 11) were infused with angiotensin (Ang) II (1000 ng/kg/min; Calbiochem) through a subcutaneous minipump for 4 weeks. As expected, this led to suprarenal AAA development and AAA rupture in a subset of animals.[40] The surviving animals after 4 weeks of Ang II infusion (n = 8) were injected with ^{99m}Tc-AGA-2 (37 ± 6 MBq) retro-orbitally under anesthesia, maintained for 1 h post injection. At 2 h post injection, the aorta and carotid arteries were dissected from the surrounding tissues and placed on a phosphor screen (MultiSensitive Phosphor Screen, PerkinElmer) along with standard references of known activity for quantitative autoradiography. The phosphor screen was scanned with a phosphorimager (Typhoon Trio, GE Healthcare Life Sciences) to obtain

https://dx.doi.org/10.1021/acs.jmedchem.0c01514
J. Med. Chem. XXXX, XXX, XXX−XXX

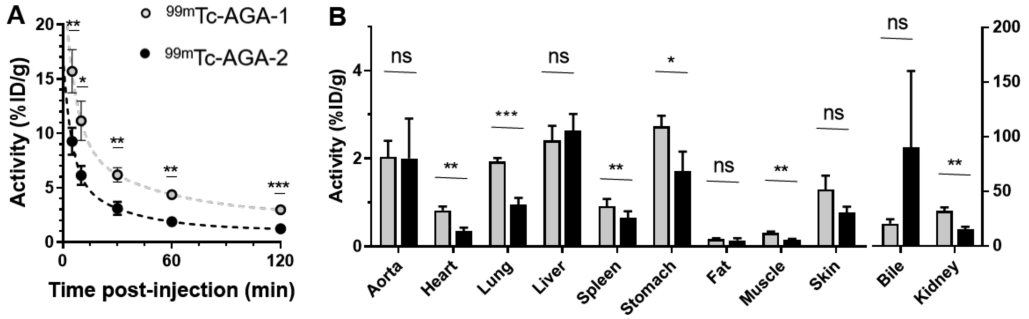

Figure 3. MMP-12 tracer biodistribution and clearance. Blood kinetics (A) and biodistribution (B) at 2 h after ^{99m}Tc-AGA-1 and ^{99m}Tc-AGA-2 administration in C57BL/6J mice. ID, injected dose. n = 3 in each group; *P < 0.05, **P < 0.01, and ***P < 0.001 (t-test).

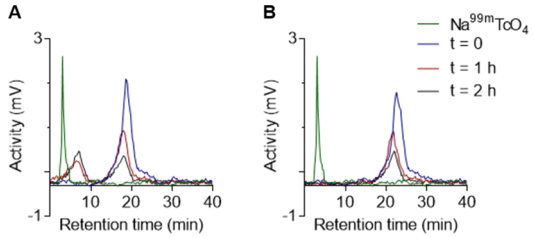

Figure 4. MMP-12 tracer stability in mouse blood. Representative radiochromatograms of $Na^{99m}TcO_4$ (green lines) and ^{99m}Tc-AGA-1 (A) and ^{99m}Tc-AGA-2 (B) immediately after radiolabeling (blue lines) after 1 h (red lines) and after 2 h (gray lines).

digitalized images of radiotracer uptake, where focal tracer uptake was readily detectable in animals with AAA (Figure 5). Regions of interest (ROIs) were drawn over different segments of the aorta to quantify the ^{99m}Tc-AGA-2 signal (Fiji/ImageJ software, NIH). This showed significantly higher ^{99m}Tc-AGA-2 uptake in the remodeled suprarenal abdominal aorta (srAA), where AAA is typically located, compared to the adjacent, normal-sized infrarenal abdominal aorta (irAA) (n = 8, P < 0.01, paired t-test, Figure 5). ^{99m}Tc-AGA-2 in suprarenal aorta was also significantly higher in Ang II-treated animals with AAA than those animals with low remodeling (LR) that had not developed AAA (n = 4 in each group, P < 0.05, Mann–Whitney U test, Figure 5).

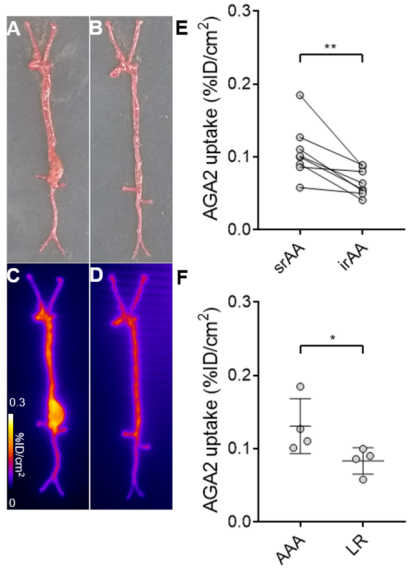

Figure 5. MMP-12 imaging in AAA. Examples of ex vivo photographs (A, B) and corresponding autoradiographs after 2 h post injection of ^{99m}Tc-AGA-2 (C, D) of aortae from Ang II-induced *Apoe*$^{-/-}$ mice with abdominal aortic aneurysm (A, C) and low remodeled aorta (B, D). (E) Quantification of the ^{99m}Tc-AGA-2 signal in suprarenal abdominal aorta (srAA) and infrarenal abdominal aorta (irAA) of Ang II-infused mice. n = 8; **P < 0.01, paired t-test. (F) Quantification of the ^{99m}Tc-AGA-2 signal in animals with AAA and low remodeled (LR) aorta. n = 4 in each group; *P < 0.05, Mann–Whitney U test. ID, injected dose.

^{99m}Tc-AGA-2 Binding Specificity. To investigate ^{99m}Tc-AGA-2 binding specificity, we evaluated the effect of MMP inhibitors on tracer binding to AAA and normal-sized irAA tissues from Ang II-infused animals, as described above. Co-incubation with 500-fold molar excess of either the panMMP inhibitor GM6001 or the MMP-12-specific inhibitor AGA significantly reduced ^{99m}Tc-AGA-2 binding to AAA tissue (P < 0.001 for both inhibitors), indicating the MMP-12-specificity of ^{99m}Tc-AGA-2 binding in AAA (Figure 6). Interestingly, co-incubation with MMP inhibitors had no effect on ^{99m}Tc-AGA-2 binding to irAA tissue, suggesting that the low level of tracer binding to the normal aorta is nonspecific (Figure 6).

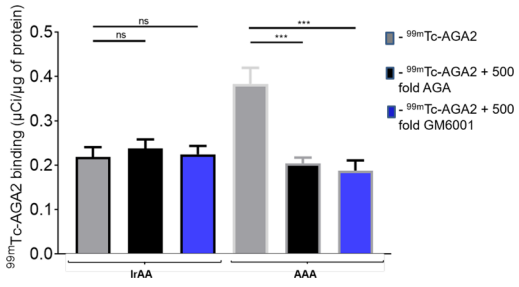

Figure 6. ^{99m}Tc-AGA-2 binding specificity. Ex vivo binding of ^{99m}Tc-AGA-2 to mouse infrarenal aorta (irAA) and AAA tissue without (gray columns) and with co-incubation with 500-fold molar excess MMP-12-specific inhibitor (AGA, yellow columns) or panMMP inhibitor (GM6001, green columns). n = 3 for each group. ns, not significant; ***P < 0.001, one-way ANOVA.

DISCUSSION AND CONCLUSIONS

Here, we report the design, synthesis, and preclinical evaluation of first generation of succinate-based hydroxamate analogues as novel selective MMP-12 inhibitors and their ^{99m}Tc-labeled HYNIC-conjugated analogues as novel MMP-12-selective SPECT radiotracers. Our data show that modifying the P3′ segment of hydroxamate MMP inhibitors with a free acid side chain leads to selective MMP-12 binding. Of the two acyclic MMP-12 tracers developed based on this

https://dx.doi.org/10.1021/acs.jmedchem.0c01514
J. Med. Chem. XXXX, XXX, XXX−XXX

design, ^{99m}Tc-AGA-2 displayed better stability and pharmacokinetics, as well as binding to human and murine AAA tissue. Autoradiography studies confirmed the higher in vivo uptake of the tracer in AAA relative to normal size aorta, setting the stage for future SPECT studies.

MMP-12 plays a key role in several inflammatory diseases such as chronic obstructive pulmonary disease (COPD), atherosclerosis, and AAA.[41] Considering the importance of MMP-12 in several pathophysiological processes, this study aimed at developing and evaluating novel selective MMP-12 inhibitors and their corresponding SPECT radiotracers. To date, several panMMP inhibitors and a few selective MMP inhibitors have been reported.[22,25,28,37,42−45] Among these, several are acyclic and macrocyclic hydroxamate analogues that contain a ZBG and a lipophilic side chain at the P1′ segment for interacting with the hydrophobic S1′ pocket of MMPs. Large differences in MMP bindings are observed by changing the side chain at the P1′ segment and, hence, the S1′ pocket is considered as the "selectivity pocket".[46] A few hydroxamate-based MMP inhibitors, e.g., ilomastat (GM-6001), RO-32-3555, CGS-27023A, marimastat, BB-1101, prinomastat, RO-32-3555, CGS-27023A, and batimastat (BB-94), have been evaluated as therapeutic agents. However, the clinical use of many of these inhibitors is hampered by musculoskeletal toxicity and other side effects, attributed in part to the lack of targeting specificity or selectivity, or the high concentrations of inhibitors required for the therapeutic effects.[19,47] As an alternative, more selective MMP inhibitors are under development. To access such selective inhibitors, as the structural differences between different MMP families mainly occur at the S1′ subsite, the investigators have utilized the P1′ group to introduce the inhibitor specificity.[48,49] Accordingly, a selective MMP-13 inhibitor has been developed, which is characterized by the absence of a catalytic zinc binding site and binding into the S1′ pocket while extending into an additional S1′ side pocket (S1′*).[50] Other investigators have developed thiirane-containing selective MMP-2 and MMP-9 inhibitors, which first coordinate with the active site zinc ion and exploit the deep S1′ pocket of MMP-2 and MMP-9. Considerable MMP-2 selectivity over MMP-9 was also achieved by exploiting the more constricted pocket of MMP-9 than MMP-2 and by introducing a bigger group with unfavorable steric interactions.[51] Phosphinic peptides are known to behave as potent inhibitors of zinc metalloproteases. By exploiting the phosphinic peptide chemistry, a highly selective MMP-12 inhibitor, RXP-470, has been developed.[52]

Succinyl hydroxamate-based small molecules that use the hydroxamate group as their ZBG may be considered as the most successful panMMP inhibitors. However, except for hydroxamate-based selective MMP-2 inhibitors,[53] not much work has been reported on developing single MMP-selective succinyl hydroxamate inhibitors, and specifically, there is no report of selective hydroxamate MMP-12 inhibitors to date. We sought to address this gap by modifying the P3′ segment to achieve selectivity toward a single MMP while maintaining high binding affinities. Accordingly, several succinyl hydroxamate analogues, i.e., CGA, CGA-1, AGA, AGA-1, and AGA-2, were designed and successfully synthesized by incorporating an acid side chain within the P3′ segment. The macrocyclic hydroxamate MMP-12 inhibitors, CGA and CGA-1, were synthesized starting from anti-succinate derivatives, following a synthetic strategy reported previously with some modifications.[33] The synthesis of the intermediate **7** was achieved according to the literature and coupling of *o*-benzyl hydroxamate to the free acid followed by deprotection of both benzyl groups resulted in CGA. To synthesize CGA-1, a di-protected glutamate was added to CGA, followed by deprotection of both ester groups. The strategy used for the synthesis of the acyclic AGA followed a previously reported synthetic methodology with modifications.[36] The intermediate **15** was synthesized starting from 4-methylvaleric acid and *S*-4-benzyl-2-oxazolidinone. The hydrolysis of ester and coupling of *o*-benzyl hydroxamate to the free acid followed by deprotection of both benzyl groups resulted in AGA. AGA-1 was synthesized using a multiprotected glutamate with a selective deprotection strategy and addition of HYNIC at the end, as shown above. AGA-2 was synthesized by replacing the phenylalanine ester from the AGA synthetic scheme with L-tyrosine benzyl ester. The HYNIC group was added by functionalizing the hydroxyl group on the phenyl to generate a free amine, which in turn was coupled to HYNIC acid to obtain AGA-2 through peptide coupling. The synthetic strategy introduced here is novel for this class of anti-succinate hydroxamate derivatives, where the P2′ position was used for adding an HYNIC group (a chelator for ^{99m}Tc-radiolabeling). This synthetic strategy reduced the number of synthetic steps (8 vs 13 for AGA-1 and AGA-2, respectively), increasing the yields and feasibility of synthesis. Also, this synthetic strategy allowed us to keep the free acid on the P3′ position, which resulted in better MMP-12 binding selectivity than AGA-1.

All these molecules with an acid side chain in their C-terminal end displayed selective nanomolar inhibition toward rhMMP-12. When both acid groups on the side chain of CGA-1 were replaced by amide groups, the resulting molecule (RYM) lost its selectivity toward MMP-12 and displayed nanomolar inhibition toward all the rhMMPs tested. Hence, it is understood that the presence of an acid side chain around the P3′ segment of succinyl hydroxamate analogues is one of the key reasons for achieving MMP-12 selectivity. Such an impact was rather unexpected in hydroxamate series but was, however, consistent with previous observations made on selective MMP-12 inhibitors for which two glutamate residues in P3′ and P2′ positions induce a favorable MMP-12 selectivity profile.[35,52] Since the analysis of the crystal structure of those inhibitors in the interaction with MMP-12 did not reveal any specific interaction of glutamate residues within the catalytic cleft, it was postulated that the MMP-12 selectivity of those inhibitors was more likely related to the presence of two negative charges, better tolerated in the case of MMP-12 than in that of other tested MMPs. In any event, the presence of a carboxylic function in the C-terminal end of inhibitors described in the present study has significant effects on their selectivity profile, but several other structural differences must be considered. Accordingly, the ring opening from cyclic CGA to acyclic AGA inhibitor has almost no impact on binding to MMP-2 and MMP-13, while a drop in potency (10-fold) is observed for MMP-7 and MMP-12. Interestingly, further structural modifications on the AGA scaffold (AGA-1 and AGA-2) have no effect on binding to MMP-12 but impact to variable extents the inhibitors' potency toward other MMPs tested. Particularly, the position of the bulky HYNIC moiety relative to the pseudo-peptide backbone seemed to have major effects on inhibitor binding, with a conjugation of this group onto the P2′ side chain that was particularly well tolerated by MMP-12 while rejected by MMP-2/7 and MMP-13. Overall, AGA-2 that combined a carboxylic function in its C-terminal

https://dx.doi.org/10.1021/acs.jmedchem.0c01514
J. Med. Chem. XXXX, XXX, XXX−XXX

end and an HYNIC moiety in its P2′ position appeared to be the most selective agent among the set of inhibitors designed in this study.

HYNIC, along with two coligands such as TPPTS and tricine, is a widely used chelator for ^{99m}Tc-labeling. Importantly, AGA and its HYNIC-conjugated radiolabeling precursors AGA-1 and AGA-2 displayed a selective inhibition profile toward MMP-12. This demonstrated that adding an HYNIC moiety does not have a significant effect on MMP-12 binding and inhibition. This confirmed previous results with a C-terminal extension on the pseudo-peptide scaffold that did not significantly impact the MMP-12 selectivity profile of optical probes or radiotracers compared to their parent molecule.[25,28,54] Both AGA-1 and AGA-2 were conveniently radiolabeled with ^{99m}Tc using TPPTS and tricine formulation in high radiochemical purity and yield to access ^{99m}Tc-AGA-1 and ^{99m}Tc-AGA-2.

MMP-12 gene expression is significantly upregulated in human AAA and both ^{99m}Tc-AGA-1 and ^{99m}Tc-AGA-2 displayed higher binding to human AAA than normal aortic tissue. The stability studies performed in murine blood revealed that ^{99m}Tc-AGA-1 is not stable and disintegrates over time, whereas ^{99m}Tc-AGA-2 was found to be stable at least for 2 h. From the biodistribution studies, we found that tracer ^{99m}Tc-AGA-2 clears faster from the blood when compared to ^{99m}Tc-AGA-1 (1.2 ± 0.2 and 3.0 ± 0.2 %ID/mL, respectively). Based on favorable blood kinetics and stability in murine blood, ^{99m}Tc-AGA-2 was chosen for further evaluation. For preclinical evaluation of our new tracers, we used an established animal model of AAA with significant upregulation of MMP-12 in aneurysm, i.e., *Apoe*$^{-/-}$ mice infused with Ang II.[40] In vivo evaluation of ^{99m}Tc-AGA-2 in Ang II-infused mice revealed significantly higher tracer uptake in AAA, where MMP-12 expression is upregulated. Blocking experiments with panMMP and MMP-12 inhibitors performed with mouse tissues established the MMP-12 specific binding of ^{99m}Tc-AGA-2 in AAA by reducing tracer binding in AAA to the nonspecific low levels observed in normal aortae. Combined, these data support the potential of ^{99m}Tc-AGA-2 for molecular imaging of MMP-12 activation, not only in AAA, but also other diseases that are associated with MMP-12 upregulation.

In conclusion, this study reports the development and evaluation of novel succinyl hydroxamate-based selective MMP-12 inhibitors and their corresponding ^{99m}Tc-labeled radiotracers. MMP-12 selectivity was achieved by introducing an acid around the P3′ segment of succinyl hydroxamate analogues. The lead tracer ^{99m}Tc-AGA-2 has favorable pharmacokinetics for vascular imaging and binds selectively to murine AAA in vivo. This sets the stage for future in vivo SPECT imaging studies in AAA and other inflammatory diseases where MMP-12 plays a key role.

■ EXPERIMENTAL SECTION

Commercially available reagents and solvents were purchased from Sigma-Aldrich (USA) and used as received without further purification. The following instruments were used for quality control: (1) HPLC: Waters HPLC system 2489, UV−Vis detector, 600 controller, and Empower Pro software; (2) LC−MS: Agilent LC−MS 6120B Quadrupole, 6550A iFunnel Q-TOF; (3) HRMS: Agilent QToF 6546 instrument (over 30,000 resolution at ∼200 MW) was used with a gradual increase in buffer composition of 0−80% MeOH in water in 10 min; (4) NMR: Agilent NMR DD2 400 MHz with OneProbe (Agilent Technologies, Santa Clara, CA, USA); (5) fluorescent plate reader (BioTek/Synergy HT). The identity and purity of the final compounds and key intermediates were assessed by analytical HPLC (see the Supporting Information for representative chromatograms) and HRMS and ^{1}H NMR (see the Supporting Information for the representative HRMS and NMR spectra). Each final compound displayed a purity of >95%.

Synthetic Chemistry. *Intermediate* ***6***. One gram (1.65 mmol) of **5** was dissolved in 20 mL of acetonitrile, 1.9 g (5.96 mmol) of Cs_2CO_3 was added, and the mixture was stirred at room temperature for 6 h. The solution was concentrated, 50 mL of water was added, and the solution was extracted with ethyl acetate (50 mL × 3). The combined organic layers were dried over $MgSO_4$, filtered, concentrated, and purified by flash column chromatography to give 460 mg (55%) of the title compound. ES−MS: observed $[MH]^+$, 524.2.

^{1}H NMR (400 MHz, chloroform-*d*) δ 7.99 (dt, 1H), 7.62−7.47 (m, 2H), 7.43−7.28 (m, 6H), 7.02−6.91 (m, 2H), 6.80−6.71 (m, 2H), 6.05 (d, 1H), 5.24−4.93 (m, 3H), 4.47−4.26 (m, 2H), 3.18 (dd, 1H), 3.04−2.78 (m, 3H), 2.35 (dtd, 2H), 1.77−1.61 (m, 3H), 1.42 (s, 10H), 1.15 (dtd, 1H), 1.00 (ddd, 1H), 0.81 (dd, 6H) (Figure S2).

Intermediate ***7***. Two hundred fifty milligrams of **6** was dissolved in 4 mL of TFA and 1 mL of DCM. After stirring at room temperature for 2 h, the solution was concentrated and dried under vacuum to get the title compound in a quantitative yield. ES−MS: observed $[MH]^+$, 468.2.

Intermediate ***8***. A mixture of **7** (220 mg, 0.47 mmol), (2-(1*H*-benzotriazol-1-yl)-1,1,3,3-tetramethyluronium hexafluorophosphate (HBTU) (214 mg, 0.56 mmol), and DIEA (0.4 mL, 2.35 mmol) was dissolved in 2.5 mL of anhydrous DMF. The mixture was stirred at room temperature for 20 min, followed by addition of Bn-ONH_2 (247.0 mg, 1.55 mmol). The mixture was further stirred at room temperature for 18 h. Twenty-five milliliters of cold H_2O was added, the mixture was stirred, and the solid formed was filtered. The solid was vacuum-dried and used for the next step. Yield, 165 mg (62%); ES−MS: observed $[MH]^+$, 573.2. ^{1}H NMR (400 MHz, chloroform-*d*) δ 7.60−7.28 (m, 10H), 6.95 (dt, 2H), 6.81−6.67 (m, 2H), 5.32−4.94 (m, 4H), 4.51−4.32 (m, 2H), 3.53−3.32 (m, 2H), 2.43−2.24 (m, 2H), 1.87−1.47 (m, 6H), 1.47−1.30 (m, 2H), 1.22−0.98 (m, 1H), 0.86 (td, 6H) (Figure S3).

Intermediate ***9*** *(CGA)*. A mixture of **8** (100 mg, 0.17 mmol) and Pd/C (0.02 g, 20%, wet) in 10 mL of methanol was stirred under hydrogen gas at room temperature for 2 h. The mixture was filtered, followed by washing of Pd/C with methanol (5 mL × 4). The combined methanol filtrate was concentrated, and the product was further purified by flash column chromatography to give 40 mg (58%) of the title compound. ES−MS: observed $[M - H]^-$, 391.2. ^{1}H NMR (400 MHz, DMSO-d_6) δ 10.33 (s, 1H), 8.67 (s, 1H), 7.73 (d, 1H), 7.21−6.96 (m, 3H), 6.79 (dd, 1H), 4.70 (s, 1H), 4.09 (s, 3H), 2.07−1.91 (m, 1H), 1.69−1.55 (m, 1H), 1.39−1.10 (m, 4H), 0.89−0.66 (m, 6H) (Figures S4 and S5).

Intermediate ***10***. To a stirred solution of **9** (30 mg, 0.07 mmol) in 1 mL of anhydrous DMF were added EDCI (30 mg, 0.157 mmol), HOBT (22 mg, 0.157 mmol), and L-glutamic acid di-*tert*-butyl ester (40 mg, 0.157 mmol), and the mixture was stirred at room temperature overnight. To the resulting mixture, ice-cold water (100 mL) was added and the mixture was stirred for 30 min. The resulting solid was filtered, dried, and purified by chromatography (silica gel, 5% methanol/DCM) to obtain 12 mg (25%) of the title compound. ES−MS: observed $[MH]^+$, 634.2.

Intermediate ***11*** *(CGA-1)*. A mixture of **10** (12 mg, 0.018 mmol) in 100 mL of DCM was cooled down to 0 °C and 20 mL of TFA was added dropwise. The mixture was stirred for 2 h at room temperature and concentrated under vacuum to remove the solvent and excess TFA. The reaction mixture was further dried by codistilling with toluene twice (10 mL × 2) and purified by preparative HPLC. ES−MS: observed $[M - H]^-$, 520.2. ^{1}H NMR (400 MHz, DMSO-d_6) δ 10.34 (s, 1H), 8.68 (s, 1H), 7.92 (d, 1H), 7.51 (d, 1H), 7.29−6.97 (m, 3H), 6.82 (dd, 1H), 6.56 (s, 1H), 4.74 (ddd, 1H), 4.28−3.92 (m, 4H), 2.27 (q, 2H), 2.00 (td, 1H), 1.92−1.75 (m, 2H), 1.60 (td, 1H), 1.44−1.04 (m, 4H), 0.89−0.53 (m, 6H) (Figures S6 and S7).

https://dx.doi.org/10.1021/acs.jmedchem.0c01514
J. Med. Chem. XXXX, XXX, XXX−XXX

Intermediate ***16***. Five hundred milligrams of **15** was dissolved in 4 mL of TFA and 5 mL of DCM. After stirring at room temperature for 2 h, the solution was concentrated and dried under vacuum to get the title compound in a quantitative yield. ES−MS: observed $[MH]^+$, 412.2.

Intermediate ***17***. A mixture of **16** (180 mg, 0.42 mmol), benzotriazol-1-yloxytris(dimethylamino)phosphonium hexafluorophosphate (BOP) (0.22 g, 0.506 mmol), and DIEA (290 mg, 1.68 mmol) was dissolved in 4 mL of anhydrous DMF. The mixture was stirred at room temperature for 20 min, followed by addition of Bn-ONH_2 (62 mg, 0.506 mmol). The mixture was further stirred at room temperature overnight and concentrated. The residue was triturated with 1 N HCl, and the solid obtained was filtered and washed with 1 N Na_2CO_3, water, and brine. The product was further purified by flash column chromatography to give 180 g (80%) of the title compound. ES−MS: observed $[MH]^+$, 517.2.

Intermediate ***18*** *(AGA)*. A mixture of **17** (100 mg, 0.193 mmol) and Pd/C (0.01 g, 10%, wet) in 10 mL of methanol was stirred under hydrogen gas at room temperature for 2 h. The mixture was filtered, followed by washing of Pd/C with methanol (5 mL × 4). The combined methanol filtrate was concentrated, and the product was further purified by flash column chromatography to give 40 mg (62%) of the title compound. ES−MS: observed $[M - H]^-$, 335.1. The representative NMR and HRMS spectra are shown in the Supporting Information. ^{1}H NMR (400 MHz, methanol-d_4) δ 7.35−7.16 (m, 5H), 4.75−4.62 (m, 1H), 3.21 (dd, 1H), 3.10−2.94 (m, 1H), 2.94−2.74 (m, 1H), 2.05 (qd, 2H), 1.53 (ddt, 2H), 1.11 (ddt, 1H), 0.88 (dd, 6H) (Figures S8 and S9).

Intermediate ***19***. To a stirred solution of Fmoc-Glu(*O*-Bn)-OH (2.0 g, 4.35 mmol), HOBT (0.7 g, 5.22 mmol), and *N*-Boc-ethylenediamine (0.77 g, 4.79 mmol) in 20 mL of anhydrous DMF cooled in an ice bath was added EDCI (1 g, 5.224 mmol), and the mixture was stirred at room temperature for 2.5 h. Ice-cold water was added to the resulting mixture, the mixture was stirred, and the solid obtained was filtered. The resulting residue was purified by chromatography (silica gel, 60% ethyl acetate/hexane) to obtain 1.8 g (72%) of the title compound. ES−MS: observed $[MH]^+$, 602.2. ^{1}H NMR (400 MHz, chloroform-*d*) δ 7.81−7.60 (m, 2H), 7.51 (d, 2H), 7.38−7.18 (m, 9H), 5.11−4.97 (m, 2H), 4.33 (q, 2H), 4.13 (t, 2H), 3.43−3.04 (m, 4H), 2.57−2.26 (m, 2H), 2.20−1.99 (m, 1H), 2.00−1.82 (m, 1H), 1.34 (s, 9H) (Figure S10).

Intermediate ***20***. One gram of **19** obtained above was dissolved in 10 mL of DCM and 3 mL of piperidine. The mixture was stirred at room temperature for 30 min and concentrated under vacuum. The product was purified by flash column chromatography (2% methanol/DCM) to give the title compound (0.6 g, 72%). ES−MS: observed $[MH]^+$, 502.2. ^{1}H NMR (400 MHz, methanol-d_4) δ 7.91−7.53 (m, 5H), 7.49−7.20 (m, 8H), 5.14 (s, 2H), 4.53−4.40 (m, 1H), 4.37 (dd, 1H), 4.24 (dt, 1H), 4.09 (dd, 1H), 3.59−3.37 (m, 3H), 3.17−2.94 (m, 2H), 2.44 (dt, 2H), 2.22−2.04 (m, 1H), 2.05−1.86 (m, 1H) (Figure S11).

Intermediate ***21***. To a stirred solution of **20** (100 mg, 0.2 mmol) in 1 mL of anhydrous DMF were added EDCI (40 mg, 0.24 mmol), HOBT (32 mg, 0.24 mmol), and 6-Boc-hydrazinonicotinic acid (50 mg, 0.2 mmol), and the mixture was stirred at room temperature overnight. To the resulting mixture, ice-cold water (100 mL) was added and the mixture was stirred for 30 min. The resulting solid was filtered, dried, and purified by chromatography (silica gel, 1% methanol/DCM) to obtain 80 mg (55%) of the title compound. ES−MS: observed $[MH]^+$, 737.2. ^{1}H NMR (400 MHz, DMSO-d_6) δ 8.99−8.80 (m, 1H), 8.52−8.35 (m, 2H), 8.24 (s, 1H), 8.00−7.84 (m, 2H), 7.79 (d, 2H), 7.63 (t, 2H), 7.49−7.38 (m, 1H), 7.37−7.15 (m, 9H), 6.52 (dd, 1H), 4.99 (s, 2H), 4.31−4.06 (m, 3H), 3.90 (td, 1H), 2.47 (d, 7H), 2.29 (t, 2H), 1.87 (ddd, 1H), 1.79−1.64 (m, 1H), 1.33 (s, 9H) (Figure S12).

Intermediate ***22***. Eighty milligrams of **21** obtained above was dissolved in 10 mL of DCM and 3 mL of piperidine. The mixture was stirred at room temperature for 30 min and concentrated under vacuum. The product was purified by flash column chromatography (2% methanol/DCM) to give the title compound (35 mg, 65%). ES−MS: observed $[MH]^+$, 515.2. ^{1}H NMR (400 MHz, methanol-d_4) δ 8.55 (dd, 2H), 8.27−8.12 (m, 1H), 8.02 (dd, 1H), 7.44−7.27 (m, 2H), 6.71 (dd, 2H), 4.17 (dd, 2H), 3.72−3.37 (m, 9H), 2.59−2.20 (m, 7H), 2.18−2.00 (m, 3H), 1.50 (s, 9H) (Figure S13).

Intermediate ***23***. A mixture of **18** (20 mg, 0.06 mmol), **22** (37 mg, 0.07 mmol), and HOBT (10 mg, 0.07 mmol) was dissolved in 2 mL of DMF and cooled down to 0−5 °C in an ice bath, followed by addition of EDCI (14 mg, 0.07 mmol). The mixture was stirred at room temperature overnight and concentrated. The residue was dissolved in 10 mL of CH_2Cl_2 and washed with 1 N HCl, H_2O, and brine. The DCM solution was dried over $MgSO_4$, filtered, and concentrated. The product was purified by flash column chromatography (2% methanol/DCM) to give the title compound (21 mg, 45%). ES−MS: observed $[MH]^+$, 799.9.

Intermediate ***24*** *(AGA-1)*. Twenty milligrams of **23** was dissolved in 2 mL of TFA and 1 mL of DCM. After stirring at room temperature for 2 h, the solution was concentrated and dried under vacuum to get crude *t*-butyl-deprotected acid product. To the acid, Pd/C (4 mg, 20%, wet) in 1 mL of methanol was stirred under hydrogen gas at room temperature for 2 h. The mixture was filtered, followed by washing of Pd/C with methanol (1 mL × 4). The combined methanol filtrate was concentrated, and the product was further purified by flash column chromatography followed by preparative HPLC purification to give 2 mg (14%) of the title compound. ES−MS: observed $[MH]^+$, 643.3. ^{1}H NMR (400 MHz, chloroform-*d*) δ 7.38−7.19 (m, 6H), 6.80 (d, 2H), 6.69−6.47 (m, 2H), 5.20−4.88 (m, 2H), 4.74 (d, 3H), 2.99 (dd, 2H), 2.84 (dd, 2H), 2.65 (tt, 2H), 2.11 (ddd, 2H), 1.41 (q, 2H), 1.30−1.12 (m, 2H), 1.02 (ddd, 1H), 0.71 (m, 6H) (Figures S14 and S15).

Intermediate ***27***. A mixture of **26** (2 g, 4.7 mmol), (2-(1*H*-benzotriazol-1-yl)-1,1,3,3-tetramethyluronium hexafluorophosphate (HBTU) (2.14 g, 5.6 mmol), and DIEA (1.6 mL, 9.4 mmol) was dissolved in 20 mL of anhydrous DMF. The mixture was stirred at room temperature for 20 min, followed by addition of Bn-ONH_2 (988 mg, 6.2 mmol). The mixture was further stirred at room temperature for 18 h. Two hundred fifty milliliters of cold H_2O was added, the mixture was stirred, and the solid formed was filtered. The solid was vacuum-dried and used for the next step. Yield, 1.65 g (66%); ES−MS: observed $[MH]^+$, 533.6. ^{1}H NMR (400 MHz, methanol-d_4) δ 7.47−7.25 (m, 9H), 7.08−6.94 (m, 2H), 6.77−6.59 (m, 2H), 5.10 (d, 2H), 4.90−4.74 (m, 7H), 4.65 (dd, 1H), 3.12−2.75 (m, 3H), 2.23−1.90 (m, 2H), 1.56−1.36 (m, 2H), 1.09−1.00 (m, 1H), 0.83 (dd, 6H) (Figure S16).

Intermediate ***28***. To a stirred solution of 2-(Boc-amino)ethyl bromide (0.31 g, 1.4 mmol) and Cs_2CO_3 (0.92 g, 2.82 mmol) in 10 mL of anhydrous acetonitrile at 60 °C was added dropwise a solution of **27** (0.5 g, 0.94 mmol) in 5 mL of acetonitrile over a period of 1 h. The resulting mixture was stirred at 60 °C for another 3 h and concentrated under vacuum. The product was redissolved with ethyl acetate and filtered, followed by washing of the solid with ethyl acetate for five times (10 mL × 5). The combined ethyl acetate filtrate was washed with 1 N HCl solution, water, and brine. The ethyl acetate solution was dried over anhydrous $MgSO_4$, filtered, and concentrated. The resulting residue was purified by silica gel chromatography using (silica gel, 40% ethyl acetate/hexane) to give the product (0.4 g, 58%). ES−MS: observed $[MH]^+$, 676.3. ^{1}H NMR (400 MHz, DMSO-d_6) δ 7.47−7.18 (m, 10H), 7.15−7.08 (m, 1H), 7.03−6.93 (m, 1H), 6.87−6.71 (m, 1H), 6.67−6.62 (m, 1H), 5.18−4.96 (m, 2H), 4.90−4.67 (m, 2H), 4.51−4.37 (m, 1H), 3.87 (td, 1H), 3.11 (d, 1H), 3.01−2.82 (m, 2H), 2.78 (d, 1H), 1.38 (s, 9H), 1.14−1.05 (m, 1H), 0.86−0.68 (m, 6H) (Figure S17).

Intermediate ***29***. Four hundred milligrams of **28** was dissolved in 4 mL of TFA and 6 mL of DCM. After stirring at room temperature for 2 h, the solution was concentrated and dried under vacuum to get crude Boc-deprotected free amine product in quantitative amounts, which was used directly for the next step. ES−MS: observed $[MH]^+$, 576.3.

Intermediate ***30***. To a stirred solution of **29** (100 mg, 0.174 mmol) in 5 mL of anhydrous DMF were added 1-hydroxy-7-azabenzotriazole (HOAt) (47 mg, 0.35 mmol), hexafluorophosphate

https://dx.doi.org/10.1021/acs.jmedchem.0c01514
J. Med. Chem. XXXX, XXX, XXX−XXX

azabenzotriazole tetramethyl uronium (HATU) (132 mg, 0.38 mmol), 6-Boc-hydrazinonicotinic acid (88 mg, 0.35 mmol), and the mixture was stirred at room temperature overnight. To the resulting mixture, ice-cold water (50 mL) was added and the mixture was stirred for 30 min. The resulting solid was filtered, dried, and purified by chromatography (silica gel, 1% methanol/DCM) to obtain 74 mg (53%) of the title compound. ES−MS: observed $[MH]^+$, 737.2. ^{1}H NMR (400 MHz, DMSO-d_6) δ 8.96−8.28 (m, 8H), 8.01−7.73 (m, 3H), 7.48−7.03 (m, 12H), 6.83 (d, J = 8.6 Hz, 2H), 6.51 (t, J = 9.5 Hz, 2H), 5.13−4.93 (m, 3H), 4.70 (d, J = 2.9 Hz, 2H), 4.45 (q, J = 7.5, 7.0 Hz, 2H), 4.04 (t, J = 5.9 Hz, 5H), 3.80 (d, J = 7.8 Hz, 6H), 3.09 (d, J = 7.4 Hz, 2H), 2.92 (dd, J = 11.9, 7.3 Hz, 3H), 2.72 (s, 2H), 2.06 (tt, J = 14.5, 5.8 Hz, 3H), 1.45−1.35 (m, 11H), 0.85−0.60 (m, 6H) (Figure S18).

Intermediate ***31***. Fifty milligrams of **30** was dissolved in 1 mL of TFA and 2 mL of DCM. After stirring at room temperature for 2 h, the solution was concentrated and dried under vacuum to get crude Boc-deprotected free amine product in quantitative amounts, which was used directly for the next step. ES−MS: observed $[MH]^+$, 637.2.

Intermediate ***32*** *(AGA-2)*. A mixture of **31** (40 mg, 0.193 mmol) and Pd/C (0.01 g, 25%, wet) in 4 mL of methanol was stirred under hydrogen gas at room temperature for 2 h. The mixture was filtered, followed by washing of Pd/C with methanol (5 mL × 4). The combined methanol filtrate was concentrated, and the product was further purified by flash column chromatography and preparative HPLC to give 2.9 mg (9%, after two steps) of the title compound. ES−MS: observed $[MH]^+$, 530.7. ^{1}H NMR (400 MHz, methanol-d_4) δ 8.53−8.35 (m, 2H), 7.99−7.79 (m, 2H), 7.04 (dq, J = 7.0, 3.3 Hz, 2H), 6.82−6.67 (m, 2H), 6.58 (dd, J = 8.8, 6.3 Hz, 2H), 3.99 (p, J = 5.5 Hz, 2H), 3.78−3.54 (m, 3H), 3.39 (q, J = 7.0 Hz, 2H), 3.02 (d, J = 4.8 Hz, 1H), 2.87−2.75 (m, 1H), 2.65 (s, 1H), 2.23−1.93 (m, 2H), 0.86−0.56 (m, 6H) (Figures S19 and S20).

MMP Affinity Determination. The MMP inhibition constants for newly synthesized selective MMP-12 inhibitors were measured based on the kinetic effects of an inhibitor on MMP-mediated catalytic cleavage of a fluorogenic substrate, namely, Mca-Lys-Pro-Leu-Gly-Leu-Dpa-Ala-Arg-NH_2, in an assay buffer of 50 mM Tris/HCl buffer (pH 6.8) and 10 mM $CaCl_2$ at 25 °C. The inhibition constants were measured toward MMP-2, MMP-7, MMP-9, MMP-12, and MMP-13 using 0.2−0.5 nM MMP at four different concentrations of the fluorogenic substrate (8, 16, 32, and 64 μM) and at five different concentrations of the inhibitors (31.25, 125, 0.5, 2.5, and 5 μM). The assays were performed in black flat-bottom 96-well plates (Microfluor 1 Black, Thermo Fisher Scientific). The fluorescence signals were monitored using a BioTek Synergy HT spectrophotometer equipped with a plate shaker and temperature device controller. From the fluorescence measured, the K_i values were determined using the method previously proposed by Horovitz and Leviski.[55]

Radiolabeling. ^{99m}Tc-labeling of precursors AGA-1 and AGA-2 was performed according to an established methodology.[37,38] Briefly, the coligand kits for radiolabeling of HYNIC precursors with $^{99m}TcO_4^-$ were prepared by lyophilizing the solution containing tricine (6.5 mg/mL), 3,3′,3″-phosphanetriyltris(benzenesulfonic acid) trisodium salt (TPPTS) (5.0 mg/mL), pluronic F-127 (0.1 mg/mL), succinic acid (12.7 mg/mL), sodium succinate (38.5 mg/mL), and mannitol (40 mg/mL).[33] Each kit was mixed with 2 μg (in 2 μL of DMSO) of HYNIC precursor (AGA-1 or AGA-2) and 200−400 μL (740−1110 MBq) of $^{99m}TcO_4^-$ solution and heated at 95 °C for 20 min. The radiolabeled solution was cooled down to room temperature before subjecting it to quality control by instant thin-layer chromatography (ITLC) and radio high-performance liquid chromatography (HPLC) analyses. ITLC analysis was performed using either a silica gel plate or TLC paper as the stationary phase and acetonitrile as the mobile phase. HPLC analysis was performed using a C-18 reverse-phase analytical column as the stationary phase and aqueous acetonitrile (containing 0.16% ammonium formate) and water (containing 0.16% ammonium formate) as the mobile phase for gradient elution.

Tracer Binding to Human Tissues. Human tissues were collected from anonymous donors under a protocol approved by the Yale University institutional review board (#12481). Frozen tissue sections of human AAA and normal aorta were incubated in triplicates with ∼1.8 MBq of ^{99m}Tc-AGA-1 or ^{99m}Tc-AGA-2 at 37 °C for 2 h. Following washing of the unbound radiotracer, the bound activity in each sample was measured using a gamma counter (WIZARD2, PerkinElmer). Next, 200 μL of protein lysis buffer [0.3 M NaCl, 50 mM Tris, 1% Triton X-100, and cOmplete Protease Inhibitor Cocktail (Sigma-Aldrich)] was added to each sample, aortic tissue was lysed, and protein concentration was measured using a colorimetric assay [Protein Assay Dye Reagent Concentrate (Bio-Rad) and BioMate 3 (Thermo Scientific)]. The bound activity in each sample was normalized to protein concentration.

■ ASSOCIATED CONTENT

Supporting Information

The Supporting Information is available free of charge at https://pubs.acs.org/doi/10.1021/acs.jmedchem.0c01514.

Inhibition constants (K_i) of CGA, CGA-1, RYM, AGA, AGA-1, and AGA-2 for recombinant murine (rm) MMP-9 and MMP-12 (Table S1); ^{1}H NMR assignments of compound **6** (Table S2); ^{1}H NMR assignments of compound **8** (Table S3); ^{1}H NMR assignments of compound CGA (Table S4); ^{1}H NMR assignments of compound CGA-1 (Table S5); ^{1}H NMR assignments of compound AGA (Table S6); ^{1}H NMR assignments of compound intermediate **19** (Table S7); ^{1}H NMR assignments of compound intermediate **20** (Table S8); ^{1}H NMR assignments of compound intermediate **21** (Table S9); ^{1}H NMR assignments of compound intermediate **22** (Table S10); ^{1}H NMR assignments of compound AGA-1 (Table S11); ^{1}H NMR assignments of compound intermediate **27** (Table S12); ^{1}H NMR assignments of compound intermediate **28** (Table S13); ^{1}H NMR assignments of compound intermediate **30** (Table S14); ^{1}H NMR assignments of compound AGA-2 (Table S15); ^{99m}Tc-AGA-1 and ^{99m}Tc-AGA-2 stability in blood (Figure S1); ^{1}H NMR spectrum of compound **6** (Figure S2); ^{1}H NMR spectrum of compound **8** (Figure S3); ^{1}H NMR spectrum of compound CGA (Figure S4); HPLC and HRMS spectra of CGA (Figure S5); ^{1}H NMR spectrum of compound CGA-1 (Figure S6); HPLC and HRMS spectra of CGA-1 (Figure S7); ^{1}H NMR spectrum of compound AGA (Figure S8); HPLC and HRMS spectra of AGA (Figure S9); ^{1}H NMR spectrum of compound intermediate **19** (Figure S10); ^{1}H NMR spectrum of compound intermediate **20** (Figure S11); ^{1}H NMR spectrum of compound intermediate **21** (Figure S12); ^{1}H NMR spectrum of compound intermediate **22** (Figure S13); ^{1}H NMR spectrum of compound AGA-1 (Figure S14); HPLC and HRMS spectra of AGA-1 (Figure S15); ^{1}H NMR spectrum of compound intermediate **27** (Figure S16); ^{1}H NMR spectrum of compound intermediate **28** (Figure S17); ^{1}H NMR spectrum of compound intermediate **30** (Figure S18); ^{1}H NMR spectrum of compound AGA-2 (Figure S19); HPLC and HRMS spectra of AGA-2 (Figure S20) (PDF)

SMILES and K_i values of compounds (CSV)

https://dx.doi.org/10.1021/acs.jmedchem.0c01514
J. Med. Chem. XXXX, XXX, XXX−XXX

AUTHOR INFORMATION

Corresponding Author

Mehran M. Sadeghi − *Cardiovascular Molecular Imaging Laboratory, Section of Cardiovascular Medicine and Yale Cardiovascular Research Center, Yale University School of Medicine, New Haven, Connecticut 06511, United States; Veterans Affairs Connecticut Healthcare System, West Haven, Connecticut 06516, United States;* orcid.org/0000-0002-5074-3510; Phone: 203 737 6954; Email: mehran.sadeghi@yale.edu; Fax: 203 937 3884

Authors

Kiran Gona − *Cardiovascular Molecular Imaging Laboratory, Section of Cardiovascular Medicine and Yale Cardiovascular Research Center, Yale University School of Medicine, New Haven, Connecticut 06511, United States; Veterans Affairs Connecticut Healthcare System, West Haven, Connecticut 06516, United States*

Jakub Toczek − *Cardiovascular Molecular Imaging Laboratory, Section of Cardiovascular Medicine and Yale Cardiovascular Research Center, Yale University School of Medicine, New Haven, Connecticut 06511, United States; Veterans Affairs Connecticut Healthcare System, West Haven, Connecticut 06516, United States*

Yunpeng Ye − *Cardiovascular Molecular Imaging Laboratory, Section of Cardiovascular Medicine and Yale Cardiovascular Research Center, Yale University School of Medicine, New Haven, Connecticut 06511, United States; Veterans Affairs Connecticut Healthcare System, West Haven, Connecticut 06516, United States*

Nowshin Sanzida − *Cardiovascular Molecular Imaging Laboratory, Section of Cardiovascular Medicine and Yale Cardiovascular Research Center, Yale University School of Medicine, New Haven, Connecticut 06511, United States; Veterans Affairs Connecticut Healthcare System, West Haven, Connecticut 06516, United States*

Arvene Golbazi − *Cardiovascular Molecular Imaging Laboratory, Section of Cardiovascular Medicine and Yale Cardiovascular Research Center, Yale University School of Medicine, New Haven, Connecticut 06511, United States; Veterans Affairs Connecticut Healthcare System, West Haven, Connecticut 06516, United States*

Parnaz Boodagh − *Cardiovascular Molecular Imaging Laboratory, Section of Cardiovascular Medicine and Yale Cardiovascular Research Center, Yale University School of Medicine, New Haven, Connecticut 06511, United States; Veterans Affairs Connecticut Healthcare System, West Haven, Connecticut 06516, United States*

Mani Salarian − *Cardiovascular Molecular Imaging Laboratory, Section of Cardiovascular Medicine and Yale Cardiovascular Research Center, Yale University School of Medicine, New Haven, Connecticut 06511, United States; Veterans Affairs Connecticut Healthcare System, West Haven, Connecticut 06516, United States*

Jae-Joon Jung − *Cardiovascular Molecular Imaging Laboratory, Section of Cardiovascular Medicine and Yale Cardiovascular Research Center, Yale University School of Medicine, New Haven, Connecticut 06511, United States; Veterans Affairs Connecticut Healthcare System, West Haven, Connecticut 06516, United States*

Saranya Rajendran − *Cardiovascular Molecular Imaging Laboratory, Section of Cardiovascular Medicine and Yale Cardiovascular Research Center, Yale University School of Medicine, New Haven, Connecticut 06511, United States; Veterans Affairs Connecticut Healthcare System, West Haven, Connecticut 06516, United States*

Gunjan Kukreja − *Cardiovascular Molecular Imaging Laboratory, Section of Cardiovascular Medicine and Yale Cardiovascular Research Center, Yale University School of Medicine, New Haven, Connecticut 06511, United States; Veterans Affairs Connecticut Healthcare System, West Haven, Connecticut 06516, United States*

Terence L. Wu − *Yale West Campus Analytical Core, Yale University, West Haven, Connecticut 06516, United States*

Laurent Devel − *CEA, INRAE, Medicaments et Technologies pour la Sante (MTS), SIMoS, Université Paris-Saclay, 91191 Gif-sur-Yvette, France;* orcid.org/0000-0002-4464-5826

Complete contact information is available at: https://pubs.acs.org/10.1021/acs.jmedchem.0c01514

Notes

The authors declare no competing financial interest.

ACKNOWLEDGMENTS

This work was supported by NIH grant R01HL138567 and VA Merit grant I01BX004038. P.B. and M.S. were supported by NIH training grants (5T32HL98069 and 5T32HL007950). We thank Dr. Mousumi Ghosh for the assistance in chemical analyses. The resources of the Yale Translational Research Imaging Center, funded in part by NIH grant 1S10RR018039, and West Campus Analytical Core at Yale University were used for these studies.

ABBREVIATIONS

AAA, abdominal aortic aneurysm; ECM, extracellular matrix; TIMP, tissue inhibitors of metalloproteinases; srAA, suprarenal abdominal aorta; irAA, infrarenal abdominal aorta; ZBG, zinc binding group; EDC-I, 1-ethyl-3-(3-dimethylaminopropyl) carbodiimide; HOBT, 1-hydroxybenzotriazole hydrate; RT, room temperature; pivCl, pivaloyl chloride; BOP, benzotriazol-1-yloxytris(dimethylamino)phosphonium hexafluorophosphate; DIEA, *N*,*N*-diisopropylethylamine; HATU, hexafluorophosphate azabenzotriazole tetramethyl uranium; HOAT, 1-hydroxy-7-azabenzotriazole; rh, recombinant human; Bq, becquerel; ID, injected dose; Ang II, angiotensin II; ROI, region of interest; TPPTS, 3,3′,3″-phosphanetriyltris-(benzenesulfonic acid) trisodium salt; HYNIC, 6-hydrazinonicotinyl

REFERENCES

(1) Nagase, H. *Zinc metalloproteases in health and disease*; London: Taylor & Francis: 1996, 153−204.

(2) Paiva, K. B. S.; Granjeiro, J. M. Bone tissue remodeling and development: focus on matrix metalloproteinase functions. *Arch. Biochem. Biophys.* **2014**, *561*, 74−87.

(3) Tomlinson, M. L.; Garcia-Morales, C.; Abu-Elmagd, M.; Wheeler, G. N. Three matrix metalloproteinases are required in vivo for macrophage migration during embryonic development. *Mech. Dev.* **2008**, *125*, 1059−1070.

(4) Werb, Z.; Chin, J. R. Extracellular Matrix remodeling during morphogenesisa. *Ann. N. Y. Acad. Sci.* **2006**, *857*, 110−118.

(5) Bottomley, K. M.; Johnson, W. H.; Walter, D. S. Matrix metalloproteinase inhibitors in arthritis. *J. Enzyme Inhib.* **1998**, *13*, 79−101.

(6) Jabłońska-Trypuć, A.; Matejczyk, M.; Rosochacki, S. Matrix metalloproteinases (MMPs), the main extracellular matrix (ECM)

enzymes in collagen degradation, as a target for anticancer drugs. *J. Enzyme Inhib. Med. Chem.* **2016**, *31*, 177−183.
(7) Kuzuya, M.; Nakamura, K.; Sasaki, T.; Wu Cheng, X.; Itohara, S.; Iguchi, A. Effect of MMP-2 deficiency on atherosclerotic lesion formation in apoE-deficient mice. *Arterioscler., Thromb., Vasc. Biol.* **2006**, *26*, 1120−1125.
(8) Li, H.; Simon, H.; Bocan, T. M. A.; Peterson, J. T. MMP/TIMP expression in spontaneously hypertensive heart failure rats: the effect of ACE-and MMP-inhibition. *Cardiovasc. Res.* **2000**, *46*, 298−306.
(9) Nygårdas, P. T.; Hinkkanen, A. E. Up-regulation of MMP-8 and MMP-9 activity in the BALB/c mouse spinal cord correlates with the severity of experimental autoimmune encephalomyelitis. *Clin. Exp. Immunol.* **2002**, *128*, 245−254.
(10) Rayment, E. A.; Upton, Z.; Shooter, G. K. Increased matrix metalloproteinase-9 (MMP-9) activity observed in chronic wound fluid is related to the clinical severity of the ulcer. *Br. J. Dermatol.* **2008**, *158*, 951−961.
(11) Steinmann-Niggli, K.; Ziswiler, R.; Küng, M.; Marti, H.-P. Inhibition of matrix metalloproteinases attenuates anti-Thy1. 1 nephritis. *J. Am. Soc. Nephrol.* **1998**, *9*, 397−407.
(12) Van Linthout, S.; Seeland, U.; Riad, A.; Eckhardt, O.; Hohl, M.; Dhayat, N.; Richter, U.; Fischer, J. W.; Böhm, M.; Pauschinger, M.; Schultheiss, H.-P.; Tschöpe, C. Reduced MMP-2 activity contributes to cardiac fibrosis in experimental diabetic cardiomyopathy. *Basic Res. Cardiol.* **2008**, *103*, 319−327.
(13) Lee, R.; Kermani, P.; Teng, K. K.; Hempstead, B. L. Regulation of cell survival by secreted proneurotrophins. *Science* **2001**, *294*, 1945−1948.
(14) Van Lint, P.; Libert, C. Chemokine and cytokine processing by matrix metalloproteinases and its effect on leukocyte migration and inflammation. *J. Leukocyte Biol.* **2007**, *82*, 1375−1381.
(15) Yamamoto, M.; Hirayama, R.; Naruse, K.; Yoshino, K.; Shimada, A.; Inoue, S.; Kayagaki, N.; Yagita, H.; Okumura, K.; Ikeda, S. Structure-activity relationship of hydroxamate-based inhibitors on membrane-bound Fas ligand and TNF-alpha processing. *Drug Des. Discovery* **1999**, *16*, 119−130.
(16) Hu, J.; Van den Steen, P. E.; Sang, Q.-X. A.; Opdenakker, G. Matrix metalloproteinase inhibitors as therapy for inflammatory and vascular diseases. *Nat. Rev. Drug Discovery* **2007**, *6*, 480−498.
(17) Cawston, T. E. Metalloproteinase inhibitors and the prevention of connective tissue breakdown. *Pharmacol. Ther.* **1996**, *70*, 163−182.
(18) Liedtke, W.; Cannella, B.; Mazzaccaro, R. J.; Clements, J. M.; Miller, K. M.; Wucherpfenning, K. W.; Gearing, A. J. H.; Raine, C. S. Effective treatment of models of multiple sclerosis by matrix metalloproteinase inhibitors. *Ann. Neurol.* **1998**, *44*, 35−46.
(19) Winer, A.; Adams, S.; Mignatti, P. Matrix metalloproteinase inhibitors in cancer therapy: Turning past failures into future successes. *Mol. Cancer Ther.* **2018**, *17*, 1147−1155.
(20) Golestani, R.; Razavian, M.; Ye, Y.; Zhang, J.; Jung, J. J.; Toczek, J.; Gona, K.; Kim, H. Y.; Elias, J. A.; Lee, C. G.; Homer, R. J.; Sadeghi, M. M. Matrix metalloproteinase-targeted imaging of lung inflammation and remodeling. *J. Nucl. Med.* **2017**, *58*, 138−143.
(21) Matusiak, N.; van Waarde, A.; Bischoff, R.; Oltenfreiter, R.; van de Wiele, C.; Dierckx, R. A. J. O.; Elsinga, P. H. Probes for non-invasive matrix metalloproteinase-targeted imaging with PET and SPECT. *Curr. Pharm. Des.* **2013**, *19*, 4647−4672.
(22) Toczek, J.; Ye, Y.; Gona, K.; Kim, H. Y.; Han, J.; Razavian, M.; Golestani, R.; Zhang, J.; Wu, T. L.; Jung, J.-J.; Sadeghi, M. M. Preclinical evaluation of RYM1, a matrix metalloproteinase-targeted tracer for imaging aneurysm. *J. Nucl. Med.* **2017**, *58*, 1318−1323.
(23) Lagente, V.; Le Quement, C.; Boichot, E. Macrophage metalloelastase (MMP-12) as a target for inflammatory respiratory diseases. *Expert Opin. Ther. Targets* **2009**, *13*, 287−295.
(24) Longo, G. M.; Buda, S. J.; Fiotta, N.; Xiong, W.; Griener, T.; Shapiro, S.; Baxter, B. T. MMP-12 has a role in abdominal aortic aneurysms in mice. *Surgery* **2005**, *137*, 457−462.
(25) Razavian, M.; Bordenave, T.; Georgiadis, D.; Beau, F.; Zhang, J.; Golestani, R.; Toczek, J.; Jung, J.-J.; Ye, Y.; Kim, H.-Y.; Han, J.; Dive, V.; Devel, L.; Sadeghi, M. M. Optical imaging of MMP-12 active form in inflammation and aneurysm. *Sci. Rep.* **2016**, *6*, 38345−38345.
(26) Wang, Y.; Ait-Oufella, H.; Herbin, O.; Bonnin, P.; Ramkhelawon, B.; Taleb, S.; Huang, J.; Offenstadt, G.; Combadière, C.; Rénia, L.; Johnson, J. L.; Tharaux, P.-L.; Tedgui, A.; Mallat, Z. TGF-β activity protects against inflammatory aortic aneurysm progression and complications in angiotensin II-infused mice. *J. Clin. Invest.* **2010**, *120*, 422−432.
(27) Johnson, J. L.; Devel, L.; Czarny, B.; George, S. J.; Jackson, C. L.; Rogakos, V.; Beau, F.; Yiotakis, A.; Newby, A. C.; Dive, V. A selective matrix metalloproteinase-12 inhibitor retards atherosclerotic plaque development in apolipoprotein E-knockout mice. *Arterioscler., Thromb., Vasc. Biol.* **2011**, *31*, 528−535.
(28) Toczek, J.; Bordenave, T.; Gona, K.; Kim, H.-Y.; Beau, F.; Georgiadis, D.; Correia, I.; Ye, Y.; Razavian, M.; Jung, J.-J.; Lequin, O.; Dive, V.; Sadeghi, M. M.; Devel, L. Novel matrix metalloproteinase 12 selective radiotracers for vascular molecular imaging. *J. Med. Chem.* **2019**, *62*, 9743−9752.
(29) Borkakoti, N. Matrix metalloprotease inhibitors: design from structure. *Biochem. Soc. Trans.* **2004**, *32*, 17−20.
(30) Dormán, G.; Cseh, S.; Hajdú, I.; Barna, L.; Kónya, D.; Kupai, K.; Kovács, L.; Ferdinandy, P. Matrix metalloproteinase inhibitors: a critical appraisal of design principles and proposed therapeutic utility. *Drugs* **2010**, *70*, 949−964.
(31) Freskos, J. N.; Asmelash, B.; Gaston, K. R.; Karwa, A.; Marzan, T. A.; Nickols, M. A.; Rogers, T. E.; Schoenstein, T.; Sympson, C. J.; Vu, B. Design and synthesis of MMP inhibitors with appended fluorescent tags for imaging and visualization of matrix metalloproteinase enzymes. *Bioorg. Med. Chem. Lett.* **2013**, *23*, 5566−5570.
(32) Serra, P.; Bruczko, M.; Zapico, J. M.; Puckowska, A.; Garcia, M. A.; Martin-Santamaria, S.; Ramos, A.; de Pascual-Teresa, B. MMP-2 selectivity in hydroxamate-type inhibitors. *Curr. Med. Chem.* **2012**, *19*, 1036−1064.
(33) Ye, Y.; Toczek, J.; Gona, K.; Kim, H.-Y.; Han, J.; Razavian, M.; Golestani, R.; Zhang, J.; Wu, T. L.; Ghosh, M.; Jung, J.-J.; Sadeghi, M. M. Novel arginine-containing macrocyclic MMP inhibitors: Synthesis, ^{99m}Tc-labeling, and evaluation. *Sci. Rep.* **2018**, *8*, 11647.
(34) Devel, L.; Czarny, B.; Beau, F.; Georgiadis, D.; Stura, E.; Dive, V. Third generation of matrix metalloprotease inhibitors: Gain in selectivity by targeting the depth of the S1' cavity. *Biochimie* **2010**, *92*, 1501−1508.
(35) Czarny, B.; Stura, E. A.; Devel, L.; Vera, L.; Cassar-Lajeunesse, E.; Beau, F.; Calderone, V.; Fragai, M.; Luchinat, C.; Dive, V. Molecular determinants of a selective matrix metalloprotease-12 inhibitor: insights from crystallography and thermodynamic studies. *J. Med. Chem.* **2013**, *56*, 1149−1159.
(36) Rouanet-Mehouas, C.; Czarny, B.; Beau, F.; Cassar-Lajeunesse, E.; Stura, E. A.; Dive, V.; Devel, L. Zinc-metalloproteinase inhibitors: Evaluation of the complex role played by the zinc-binding group on potency and selectivity. *J. Med. Chem.* **2017**, *60*, 403−414.
(37) Razavian, M.; Zhang, J.; Nie, L.; Tavakoli, S.; Razavian, N.; Dobrucki, L. W.; Sinusas, A. J.; Edwards, D. S.; Azure, M.; Sadeghi, M. M. Molecular imaging of matrix metalloproteinase activation to predict murine aneurysm expansion in vivo. *J. Nucl. Med.* **2010**, *51*, 1107−1115.
(38) Liu, S.; Edwards, D. S.; Harris, A. R.; Ziegler, M. C.; Poirier, M. J.; Ewels, B. A.; Diluzio, W. R.; Hui, P. Towards developing a non-$SnCl_2$ formulation for RP444, a new radiopharmaceutical for thrombus imaging. *J. Pharm. Sci.* **2001**, *90*, 114−123.
(39) Curci, J. A.; Liao, S.; Huffman, M. D.; Shapiro, S. D.; Thompson, R. W. Expression and localization of macrophage elastase (matrix metalloproteinase-12) in abdominal aortic aneurysms. *J. Clin. Invest.* **1998**, *102*, 1900−1910.
(40) Daugherty, A.; Manning, M. W.; Cassis, L. A. Angiotensin II promotes atherosclerotic lesions and aneurysms in apolipoprotein E-deficient mice. *J. Clin. Invest.* **2000**, *105*, 1605−1612.
(41) Elkington, P. T.; Cooke, G. S. MMP12, lung function, and COPD in high-risk populations. *N. Engl. J. Med.* **2010**, *362*, 1241.

https://dx.doi.org/10.1021/acs.jmedchem.0c01514
J. Med. Chem. XXXX, XXX, XXX−XXX

(42) Butsch, V.; Börgel, F.; Galla, F.; Schwegmann, K.; Hermann, S.; Schäfers, M.; Riemann, B.; Wünsch, B.; Wagner, S. Design, (radio)synthesis, and in vitro and in vivo evaluation of highly selective and potent matrix metalloproteinase 12 (MMP-12) inhibitors as radiotracers for positron emission tomography. *J. Med. Chem.* **2018**, *61*, 4115−4134.
(43) Hagimori, M.; Temma, T.; Kudo, S.; Sano, K.; Kondo, N.; Mukai, T. Synthesis of radioiodinated probes targeted toward matrix metalloproteinase-12. *Bioorg. Med. Chem. Lett.* **2018**, *28*, 193−195.
(44) Kondo, N.; Temma, T.; Aita, K.; Shimochi, S.; Koshino, K.; Senda, M.; Iida, H. Development of matrix metalloproteinase-targeted probes for lung inflammation detection with positron emission tomography. *Sci. Rep.* **2018**, *8*, 1347.
(45) Su, H.; Spinale, F. G.; Dobrucki, L. W.; Song, J.; Hua, J.; Sweterlitsch, S.; Dione, D. P.; Cavaliere, P.; Chow, C.; Bourke, B. N.; Hu, X. Y.; Azure, M.; Yalamanchili, P.; Liu, R.; Cheesman, E. H.; Robinson, S.; Edwards, D. S.; Sinusas, A. J. Noninvasive targeted imaging of matrix metalloproteinase activation in a murine model of postinfarction remodeling. *Circulation* **2005**, *112*, 3157−3167.
(46) Reichelt, A.; Gaul, C.; Frey, R. R.; Kennedy, A.; Martin, S. F. Design, synthesis, and evaluation of matrix metalloprotease inhibitors bearing cyclopropane-derived peptidomimetics as P1' and P2' replacements. *J. Org. Chem.* **2002**, *67*, 4062−4075.
(47) Wojtowicz-Praga, S.; Torri, J.; Johnson, M.; Steen, V.; Marshall, J.; Ness, E.; Dickson, R.; Sale, M.; Rasmussen, H. S.; Chiodo, T. A.; Hawkins, M. J. Phase I trial of Marimastat, a novel matrix metalloproteinase inhibitor, administered orally to patients with advanced lung cancer. *J. Clin. Oncol.* **1998**, *16*, 2150−2156.
(48) Matter, H.; Schudok, M. Recent advances in the design of matrix metalloprotease inhibitors. *Curr. Opin. Drug Discovery Dev.* **2004**, *7*, 513−535.
(49) Chen, J. M.; Nelson, F. C.; Levin, J. I.; Mobilio, D.; Moy, F. J.; Nilakantan, R.; Zask, A.; Powers, R. Structure-based design of a novel, potent, and selective inhibitor for MMP-13 utilizing NMR spectroscopy and computer-aided molecular design. *J. Am. Chem. Soc.* **2000**, *122*, 9648−9654.
(50) Engel, C. K.; Pirard, B.; Schimanski, S.; Kirsch, R.; Habermann, J.; Klingler, O.; Schlotte, V.; Weithmann, K. U.; Wendt, K. U. Structural basis for the highly selective inhibition of MMP-13. *Chem. Biol.* **2005**, *12*, 181−189.
(51) Ikejiri, M.; Bernardo, M. M.; Meroueh, S. O.; Brown, S.; Chang, M.; Fridman, R.; Mobashery, S. Design, synthesis, and evaluation of a mechanism-based inhibitor for gelatinase A. *J. Org. Chem.* **2005**, *70*, 5709−5712.
(52) Devel, L.; Rogakos, V.; David, A.; Makaritis, A.; Beau, F.; Cuniasse, P.; Yiotakis, A.; Dive, V. Development of selective inhibitors and substrate of matrix metalloproteinase-12. *J. Biol. Chem.* **2006**, *281*, 11152−11160.
(53) Bencsik, P.; Kupai, K.; Görbe, A.; Kenyeres, É.; Varga, Z. V.; Pálóczi, J.; Gáspár, R.; Kovács, L.; Weber, L.; Takács, F.; Hajdú, I.; Fabó, G.; Cseh, S.; Barna, L.; Csont, T.; Csonka, C.; Dormán, G.; Ferdinandy, P. Development of matrix metalloproteinase-2 inhibitors for cardioprotection. *Front. Pharmacol.* **2018**, *9*, 296.
(54) Bordenave, T.; Helle, M.; Beau, F.; Georgiadis, D.; Tepshi, L.; Bernes, M.; Ye, Y.; Levenez, L.; Poquet, E.; Nozach, H.; Razavian, M.; Toczek, J.; Stura, E. A.; Dive, V.; Sadeghi, M. M.; Devel, L. Synthesis and in vitro and in vivo evaluation of MMP-12 selective optical probes. *Bioconjugate Chem.* **2016**, *27*, 2407−2417.
(55) Horovitz, A.; Levitzki, A. An accurate method for determination of receptor-ligand and enzyme-inhibitor dissociation constants from displacement curves. *Proc. Natl. Acad. Sci. U. S. A.* **1987**, *84*, 6654.

https://dx.doi.org/10.1021/acs.jmedchem.0c01514
J. Med. Chem. XXXX, XXX, XXX−XXX